M. Shahrbaf [1, 2], D. Blaschke [2, 3, 4, *],
A. G. Grunfeld [5, 6], H. R. Moshfegh [1]

FIRST-ORDER PHASE TRANSITION FROM HYPERNUCLEAR MATTER TO DECONFINED QUARK MATTER OBEYING NEW CONSTRAINTS FROM COMPACT STAR OBSERVATIONS

[1] University of Tehran, Tehran
[2] Institute for Theoretical Physics, University of Wroclaw, Wroclaw, Poland
[3] Joint Institute for Nuclear Research, Dubna
[4] National Research Nuclear University (MEPhI), Moscow
[5] CONICET, Buenos Aires
[6] Departamento de Física, Comisión Nacional de Energía Atómica, Buenos Aires
[*] E-mail: david.blaschke@gmail.com

Фазовый переход первого рода гиперядерной материи
в деконфинированное кварковое вещество, подчиняющееся новым
ограничениям из наблюдений компактных звезд

Мы пересматриваем проблему «гиперонной загадки» и ее предложенное решение с помощью деконфайнмента кварков в рамках двухфазного подхода с гиперядерным уравнением состояния, полученным в рамках ограниченного вариационного метода низших порядков, и жестким уравнением состояния для кваркового вещества, основанным на цветовой сверхпроводящей нелокальной модели Намбу–Йона-Лазинио с постоянными коэффициентами (модель A) и с коэффициентами, зависящими от плотности (модель B). Мы впервые вводим уравнение состояния гибридных звезд с промежуточной гиперядерной фазой между ядерной фазой и фазой кварковой материи с цветовой сверхпроводимостью (модель B), для которой максимум массы компактных звезд достигает $2{,}2M_\odot$ в соответствии с последними наблюдениями для PSR J0740 + 6620. Мы обсуждаем решения для фазового перехода в симметричном веществе с возможными приложениями в будущих программах сканирования энергии в столкновениях тяжелых ионов на установках CERN, RHIC, NICA и FAIR.

First-Order Phase Transition from Hypernuclear Matter to Deconfined
Quark Matter Obeying New Constraints from Compact Star Observations

We reconsider the problem of the "hyperon puzzle" and its suggested solution by quark deconfinement within the two-phase approach where the hypernuclear equation of state is obtained from the lowest-order constrained variational method and a rigid quark matter equation of state based on the color superconducting nonlocal Nambu–Jona-Lasinio model with constant coefficients (model A) and with density-dependent coefficients (model B). With model B we introduce for the first time an equation of state of hybrid stars with an intermediate hypernuclear phase between the nuclear and the color superconducting quark matter phases, for which the maximum mass of compact stars reaches $2.2M_\odot$ in accordance with the latest observations for PSR J0740 + 6620. We discuss phase transition solutions in symmetric matter with possible applications in future energy scan programs in heavy-ion collisions at CERN, RHIC, NICA and FAIR.

INTRODUCTION

The structure and properties of nuclear matter at supersaturation densities $n \gg n_0 \approx 0.16$ m^{-3} are still open questions affecting nuclear physics, particle physics and astrophysics. Such a state of matter is realized in the core of a neutron star (NS) and its mechanical properties, encoded in the equation of state (EoS), are uniquely related to the corresponding mass–radius relationship via the Tolman–Oppenheimer–Volkoff equations. Theoretically, one can infer from mass–radius measurements the NS EoS, see Ref. [1] for an early attempt. Because of the absence of reliable radius measurements, however, we may speak at present only about direct constraints on the EoS from observations of masses and radii of compact stars (CS). Of particular importance are constraints on the maximum mass as one characteristics of the EoS. The recent measurement of the mass $2.14^{+0.10}_{-0.09} M_\odot$ for the millisecond pulsar PSR J0740 + 6620 [2] has renewed the requirement of a sufficient stiffness of the EoS at supersaturation densities. On the other hand, the compact star radii should be in accord with the bounds on tidal deformabilities derived from the gravitational waves detected by the LIGO and Virgo Collaboration (LVC) from the inspiral phase of the binary neutron star merger GW170817 [3], for instance, $R_{1.6M_\odot} > 10.7$ km [4] and $R_{1.4M_\odot} < 13.6$ km [5]. These new observational data for masses and radii (compactness) provide more stringent constraints for the behavior of the neutron star EoS.

One of the key questions concerns the composition of NS interiors. As early as 1960 it was proposed by Ambartsumyan and Saakyan [6] that hyperons may occur in the core of an NS. This work, still before the discovery of pulsars, considered noninteracting particles. In modern calculations with realistic two-particle and three-particle interactions it was found that the appearance of hyperons softens the EoS to the extent that even the mass of typical binary radio pulsars ($\sim 1.35 M_\odot$) could not be described [7–9] (weak hyperon puzzle). The more severe "strong" hyperon puzzle consists in the fact that the observational lower bound on the value of the CS maximum mass is nowadays well above $2M_\odot$.*

---

*There are recent works suggesting many-body forces at short distances based on multi-pomeron exchange which not only improve the description of nuclear saturation properties and elastic nucleus–nucleus scattering data but also allow for an NS mass above $2M_\odot$ when including hyperons, see [10] and references therein. In relativistic mean field approaches to hypernuclear matter, the repulsive ϕ-meson mean field provides a sufficient stiffening to avoid a severe problem with the "hyperon puzzle", see [11, 12] and [13] for a recent review.

Besides hypernuclear matter, there are other non-nucleonic forms of matter possible in CS interiors, in particular for the most massive stars with highest central densities, e.g., hadronic matter with Δ isobars [14], dibaryons [15] and parity doubled states [16–18] as well as deconfined quark matter, which all may occur in the normal but also in the superconducting/superfluid state with pairing gaps in the dispersion relations. Moreover, there are meson condensates possible, see [19] and references therein. As for the change in the composition of dense NS matter, the question arises whether it will be favorable to first excite heavier hadronic species and only at still higher densities to dissociate them into a state of deconfined quark matter or whether deconfinement can occur at sufficiently low densities to circumvent the occurrence of hyperons. The latter alternative has been suggested as a possible solution to the weak hyperon puzzle in [20,21]. Since an equilibrium phase transition (PT) leads to a softening of the EoS and would have worsened the problem with the insufficient maximum mass, a strongly density-dependent stiffening of the EoS after the transition had to be introduced. To this end, in [20, 21] a density-dependent bag pressure was suggested but maximum masses stayed still well below $2M_\odot$.

There is an old controversy whether the observation of a CS with $M > 2M_\odot$ would not rule out hybrid stars with quark matter cores and thus would remove the quark deconfinement as a solution of the strong hyperon puzzle, but as could be shown, e.g., in [22], a sufficiently strong vector meson coupling would allow maximum masses of quark-hadron hybrid stars above $2M_\odot$ and the occurrence of a diquark condensate can induce a lowering of the deconfinement transition so that indeed problems with the high-density behavior of hadronic EoS like the hyperon puzzle and the direct Urca problem can be solved. Using the same three-flavor color superconducting NJL model [23] as in [22] and an extension of the density-dependent relativistic mean field model DD2 [24] to include Λ hyperons and an additional repulsive ϕ-meson mean field, it has been shown in [25] that with this setting a CS structure with a hypernuclear shell and color superconducting quark matter in the core under fulfillment of the $2M_\odot$ mass constraint is possible. For this solution it was essential to add a medium-dependent bag pressure contribution, see also [26] where a different version of a relativistic mean field theory with hyperons [27, 28] is used.

In this work, we use the lowest-order constrained variational (LOCV) method to provide an EoS for baryonic matter for different asymmetry parameters $x = (\rho_n - \rho_p)/\rho_B$ and hyperon fractions $x_\Lambda = \rho_\Lambda/\rho_B$. The LOCV approach allows us to study the PT for arbitrary isospin asymmetries.

We shall consider here the deconfinement to a recently developed stiff EoS for deconfined quark matter [29, 30], i.e., the nonlocal Nambu–Jona-Lasinio (nlNJL) model which is a modern approach to describe quark matter including color superconductivity. The PT as obtained by a Maxwell construction predicts a jump in energy density which, depending on its size, may even lead to an unstable

branch in the CS mass–radius diagram which eventually is followed by a third family branch [31] of stable hybrid stars, disconnected from the second family of pure neutron or moderate hybrid stars [32]. As an observable feature the third family leads to the mass twin phenomenon [33] which has recently been shown to be possible also for high-mass pulsars [34–36]. We will employ the interpolation method on the basis of the nlNJL EoS [30] which is a powerful and flexible tool to construct a strong PT and answer the question of the possible existence of a third family of CSs which would require a strong PT in dense matter.

In Sec. 1 we present the theoretical formulation based on the LOCV method and nlNJL model. Section 2 is devoted to the results and discussion for the properties of hypernuclear matter and hadron-quark matter PT. In Sec. 3 the properties of PT for isospin-symmetric matter as well as a comparative study on model dependence of PT are presented. This includes a discussion of the PT onset in symmetric matter that would follow from the hybrid EoS model constrained by modern NS observations. The summary and conclusions are given in the final section.

1. HYBRID STAR EOS WITH HYPERONS AND QUARK DECONFINEMENT

In this work we use a two-phase description in order to construct a transition from hadronic to the quark phase. The theoretical approaches used to calculate the EoS for each of these two phases will be discussed in the following two subsections.

1.1. Hadronic Phase: Hypernuclear Matter within the LOCV Method. For the nuclear matter phase, we use a microscopic potential-based technique called LOCV method by Owen et al. [37] for calculation of the bulk properties of nuclear fluids, such as the saturation properties. Different types of nucleon–nucleon interactions have been employed so far, such as Reid68 and Δ-Reid [38], UV14, AV14 and AV18 [39–41], and charge-dependent Reid potential (Reid93) [42, 43], while a central potential [44, 45] has been used for nucleon–hyperon and hyperon–hyperon interactions recently. Since the three-body interactions have an essential role to describe the nuclear matter properties, the LOCV method is capable of dealing with the three-body interactions like Urbana type [46] and chiral three-nucleon force [47]. This method has been used not only at zero but also at finite temperature for the calculation of thermodynamic properties of hot and cold fermionic fluids [39–41,43,48,49]. In other variational methods such as the APR method [50], while the calculations are similar to the ones in our method and there is a good agreement between our results [51], there are some differences in calculating the correlation functions. Usually, in other variational methods, several free parameters in the correlation functions are

chosen so that the energy per nucleon at every given density is minimized but they do not mention the normalization constraint and therefore it is not clear how the normalization constraint is satisfied. In the LOCV method, we impose the normalization condition by demanding the control parameter χ to vanish,

$$\chi = \langle \Psi | \Psi \rangle - 1 = \frac{1}{A} \sum_{ij} \langle ij | F_p^2 - f^2 | ij - ji \rangle = 0, \tag{1}$$

where F_p is the Pauli function. For asymmetric nuclear matter, it is defined by

$$F_p(r) = \begin{cases} \left[1 - \frac{9}{2} \left(\frac{J_1(k_{f_i} r)}{k_{f_i} r} \right)^2 \right]^{-\frac{1}{2}} & \text{indistinguishable particles,} \\ 1 & \text{distinguishable particles,} \end{cases}$$

where $J_1(k_{f_i} r)$ denotes the spherical Bessel function of order 1 and k_{f_i} is the Fermi momentum of each particle. The wave function of the system then reads

$$\Psi(1 \dots A) = F(1 \dots A) \Phi(1 \dots A), \tag{2}$$

where $\Phi(1 \dots A)$ is the uncorrelated Fermi system wave function (Slater determinant of plane waves) and $F(1 \dots A)$ is the many-body correlation function. In (2), $f(ij)$ denotes the two-body state-dependent correlation functions. In the Jastrow formalism, the two-body correlation functions $f(ij)$ are defined as

$$f(ij) = \sum_{\alpha, p=1}^{3} f_\alpha^p(ij) O_\alpha^p(ij), \tag{3}$$

where O_α^p is the projection operator which projects on to the α channels, i.e., $\alpha = \{J, L, S, T, T_z, s\}$ where s is the strangeness number of baryons. For singlet and triplet channels with $J = L$ we choose $p = 1$ and for triplet channels with $J = L \pm 1$ we set $p = 2, 3$. The operators O_α^p are given by

$$O_\alpha^{p=1-3} = 1, \left(\frac{2}{3} + \frac{1}{6} S_{12} \right), \left(\frac{1}{3} - \frac{1}{6} S_{12} \right), \tag{4}$$

where $S_{12} = 3(\sigma_1.\hat{r})(\sigma_2.\hat{r}) - \sigma_1.\sigma_2$ is the spin tensor operator with σ_1 and σ_2 describing the spins of nucleons 1 and 2, respectively. In this model, it is supposed that there is a specific form for the long-range behavior of the correlation functions due to an exact functional minimization of the two-body energy with respect to the short-range parts of the correlation functions. The constraint will be incorporated only up to a certain distance (the healing distance) where the logarithmic derivative of the correlation function matches that of the Pauli function. After the healing distance, the correlation function will be replaced with

4

the Pauli function. The condition (1) also ensures that the correlations are predominantly of the two-body kind and the higher many-body contributions are small, and results in a rapid convergence of the cluster expansion. In comparison with the mean field theories, we can directly use the realistic interactions for baryons which are phenomenologically obtained from scattering data. Of course, since the LOCV method is a non-relativistic method, when considering hyperons, our results for the NS maximum mass are well below the value required by astrophysical observations, in agreement with previous works based on Brueckner–Hartree–Fock (BHF) approach as well as other non-relativistic potential models [7–9]. In a Green function method like BHF, however, the correlation functions cannot be obtained.

We point out the following characteristics of the LOCV method:

1. A microscopic method in configuration space which is purely variational;

2. Simply generalizable to finite temperature;

3. Correlation functions for baryon–baryon interactions as well as structure functions, which are important quantities of interest in scattering studies, are obtained directly in our formulation. In fact, the two-body energy in the LOCV method is a functional of correlation function. Thus, by a minimization of the energy with respect to the correlation function, one can obtain both of the energy and correlation function;

4. Tensor correlation functions are employed;

5. Considering Eq.(4), the energy per baryon and correlation functions are state-dependent and can be obtained for each state which is defined by $\alpha = \{J, L, S, T, T_z, s\}$;

6. Numerical calculations are not time consuming, so that they can be performed on standard desktop or laptop computers.

Recently, we have extended the work of Goudarzi et al. [46] by including hyperons, and studied the composition and EoS of a charged neutral, equilibrated mixture of neutrons, protons, electrons, muons, free Σ^- as well as Λ hyperons at zero temperature. In this work, the AV18 nucleon–nucleon interaction supplemented with Urbana-type three-body force [50, 52] is employed for nucleonic part of hypernuclear matter, while hyperons are considered as non-interacting particles. The chemical potential of nucleons has been calculated within the LOCV method and the equations of β-stability in the presence of free hyperons, as well as the TOV equations for the mass–radius relation of hypernuclear stars, have been solved [9]. The results for the EoS of nuclear matter (LOCV) and hypernuclear matter (LOCVY) obtained within the LOCV method are shown in Fig. 1.

5
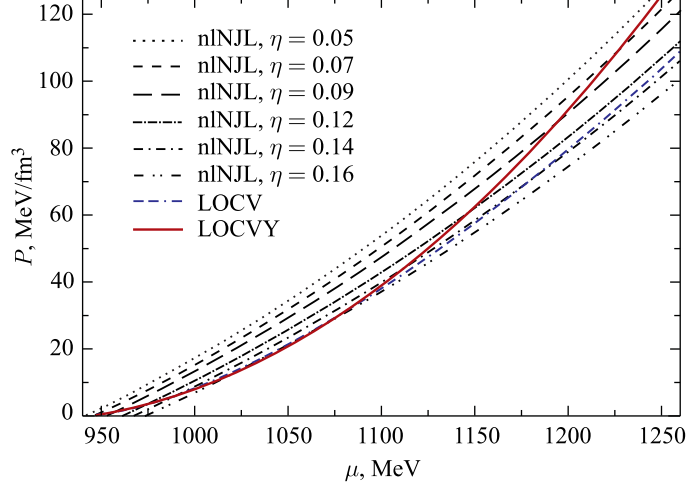
Fig. 1. Nuclear and hypernuclear matter EoS obtained from the LOCV method, compared with quark matter EoS according to the nlNJL model with color superconductivity for different values of the dimensionless vector meson coupling strength parameter η

1.2. Quark Matter EoS within nlNJL Model. For the quark matter phase we employ a color superconducting nonlocal chiral quark model of the Nambu–Jona-Lasinio type (nlNJL) for the case of two quark flavors. This model has recently been discussed in the context of modern compact star constraints in Ref. [30], where references to preceding work are also given. For the convenience of the reader, we summarize here the nlNJL approach which is characterized by four-fermion interactions in the scalar quark–antiquark, the anti-triplet scalar diquark and the vector quark–antiquark channels. The effective Euclidean action for two light flavors reads

$$S_E = \int d^4x \; \left\{ \bar{\psi}(x) \left(-i\slashed{\partial} + m_c \right) \psi(x) - \frac{G_S}{2} j_S^f(x) j_S^f(x) - \right.$$
$$\left. -\frac{H}{2} \left[j_D^a(x) \right]^\dagger j_D^a(x) - \frac{G_V}{2} j_V^\mu(x) \, j_V^\mu(x) \right\}. \qquad (5)$$

We considered the current quark mass, m_c, to be equal for u and d quarks. The nonlocal currents $j_{S,D,V}(x)$, based on a separable approximation of the effective one-gluon exchange (OGE) model of QCD, read

$$j_S^f(x) = \int d^4z \; g(z) \; \bar{\psi}\left(x + \frac{z}{2} \right) \Gamma_f \, \psi\left(x - \frac{z}{2} \right), \qquad (6)$$

$$j_D^a(x) = \int d^4z \; g(z) \; \bar{\psi}_C\left(x + \frac{z}{2} \right) \Gamma_D \, \psi\left(x - \frac{z}{2} \right), \qquad (7)$$

6

$$j_V^\mu(x) = \int d^4z \; g(z) \; \bar{\psi}\left(x + \frac{z}{2}\right) i\gamma^\mu \; \psi\left(x - \frac{z}{2}\right), \tag{8}$$

where $\psi_C(x) = \gamma_2\gamma_4 \bar{\psi}^T(x)$, $\Gamma_f = (\mathbb{1}, i\gamma_5\vec{\tau})$ and $\Gamma_D = i\gamma_5\tau_2\lambda_a$, while $\vec{\tau}$ and λ_a, with $a = 2, 5, 7$, stand for Pauli and Gell-Mann matrices acting on flavor and color spaces, respectively. The function $g(z)$ in Eqs. (8) is a covariant form factor which accounts for the nonlocality of the effective quark interactions [53].

The coupling constants ratios H/G_S, G_V/G_S are input parameters. For OGE interactions in the vacuum, Fierz transformation leads to $H/G_S = 0.75$ and $\eta = G_V/G_S = 0.5$. However, these values are subject to rather large theoretical uncertainties. In fact, thus far there is no strong phenomenological constraint on the ratio H/G_S, except for the fact that values larger than one are quite unlikely to be realized in QCD since they might lead to color symmetry breaking in the vacuum. Below, at the end of this subsection, we will consider two schemes of fixing the values of the coupling constants that will be applied in the present work.

The first one, denoted as "model A", assumes a set of coupling constants to be fixed for vacuum conditions and afterwards, at finite densities remains unchanged. The second one is denoted as "model B" and has been introduced in Ref. [30] as a generalized nlNJL model with a functional dependence of parameters on the baryochemic potential as the natural thermodynamic variable of the pressure as thermodynamic potential in the grand canonical ensemble. Before giving further details on models A and B, we describe the mean field approximation to the thermodynamic potential of the nlNJL model.

After a proper bosonization of this quark model, introducing scalar, vector, and diquark fields, we work in mean field approximation (MFA). In the diquark sector, owing to the color symmetry, one can rotate in color space to fix $\Delta_5 = \Delta_7 = 0$, $\Delta_2 = \Delta$. Finally, we consider the Euclidean action at zero temperature and finite baryon chemical potential, where we introduce six different chemical potentials μ_{fc}, depending on the two quark flavors $f = u, d$ and quark colors $c = r, g, b$.

The MFA grand canonical thermodynamic potential per unit volume can be written as

$$\Omega^{\text{MF}} = \frac{\bar{\sigma}^2}{2G_S} + \frac{\bar{\Delta}^2}{2H} - \frac{\bar{\omega}^2}{2G_V} -$$
$$- \frac{1}{2} \int \frac{d^4p}{(2\pi)^4} \; \ln\det\left[S^{-1}(\bar{\sigma}, \bar{\Delta}, \bar{\omega}, \mu_{fc})\right]. \tag{9}$$

A detailed description of the model and the explicit expression for the thermodynamic potential after calculating the determinant of the inverse of the propagator can be found in Ref. [54]. The mean field values $\bar{\sigma}$, $\bar{\Delta}$ and $\bar{\omega}$ satisfy the coupled equations

$$\frac{d\Omega^{\text{MF}}}{d\bar{\Delta}} = 0, \quad \frac{d\Omega^{\text{MF}}}{d\bar{\sigma}} = 0, \quad \frac{d\Omega^{\text{MF}}}{d\bar{\omega}} = 0. \tag{10}$$

7

As shown above, there is a freedom in choosing the direction of $\bar{\Delta}$ in color space. In the ansatz we considered, the colors participating in the pairing are r, g, leaving the blue color unpaired. When considering that our system is in chemical equilibrium, one can see that all chemical potentials are no longer independent and can be expressed in terms of three independent quantities: the baryonic chemical potential μ, a quark electric chemical potential μ_{Q_q} and a color chemical potential μ_8. The corresponding relations read

$$\mu_{ur} = \mu_{ug} = \frac{\mu}{3} + \frac{2}{3}\mu_{Q_q} + \frac{1}{3}\mu_8, \tag{11}$$

$$\mu_{ub} = \frac{\mu}{3} + \frac{2}{3}\mu_{Q_q} - \frac{2}{3}\mu_8, \tag{12}$$

$$\mu_{dr} = \mu_{dg} = \frac{\mu}{3} - \frac{1}{3}\mu_{Q_q} + \frac{1}{3}\mu_8, \tag{13}$$

$$\mu_{db} = \frac{\mu}{3} - \frac{1}{3}\mu_{Q_q} - \frac{2}{3}\mu_8, \tag{14}$$

where the chemical potential μ_{Q_q} distinguishes between up and down quarks, and the color chemical potential μ_8 has to be introduced to ensure color neutrality.

In this work we are interested in describing the behavior of quark matter in the core of NSs; therefore, we shall consider that quark matter is electrically and color neutral and in equilibrium under weak interactions. We include electrons and muons as a free relativistic Fermi gas. Beta-decay reactions read

$$d \to u + l + \bar{\nu}_l, \quad u + l \to d + \nu_l, \tag{15}$$

for $l = e, \mu$. We assume that (anti)neutrinos are no longer trapped in the stellar core. Then, we have the following relation between chemical potentials:

$$\mu_{dc} - \mu_{uc} = -\mu_{Q_q} = \mu_l \tag{16}$$

for $c = r, g, b$, $\mu_e = \mu_\mu = \mu_l$. Finally, we impose electrical and color charge neutrality conditions

$$\rho_{Q_{\text{tot}}} = \rho_{Q_q} - \sum_{l=e,\mu} \rho_l =$$

$$= \sum_{c=r,g,b} \left(\frac{2}{3}\rho_{uc} - \frac{1}{3}\rho_{dc} \right) - \sum_{l=e,\mu} \rho_l = 0, \tag{17}$$

$$\rho_8 = \frac{1}{\sqrt{3}} \sum_{f=u,d} (\rho_{fr} + \rho_{fg} - 2\rho_{fb}) = 0, \tag{18}$$

where the expressions for the lepton densities ρ_l and the quark densities ρ_{fc} can be found in the Appendix of [54].

8

Summing up, for each value of μ one obtains $\bar{\Delta}$, $\bar{\sigma}$, μ_l and μ_8 by self-consistently solving the gap equations (10), together with β-equilibrium Eq. (16) and electric and color charge neutrality Eqs. (17) and (18) conditions.

The quark matter EoS is then

$$P(\mu) = P(\mu; \eta(\mu), B(\mu)) = -\Omega^{\mathrm{MF}}(\eta(\mu)) - B(\mu), \qquad (19)$$

where for later use we allow for the possibility of a bag pressure shift B stemming, e.g., from a medium dependence of the gluon sector, and both parameters η and B may depend on the chemical potential [30].

The resulting EoS for color superconducting quark matter for different values of η is shown in Fig. 1 in comparison with the nuclear and hypernuclear ones. This quark matter model with density-independent coefficients is denoted as model A. From the crossing of the corresponding lines one can obtain the hadron-to-quark matter PT, see below.

In Ref. [30] has also been discussed the possibility of a density dependence of the vector meson coupling strength η and an additional softening of the quark matter EoS due to a confining bag function, also with a density dependence. The density dependence of these two parameters of the generalized nlNJL model has been introduced by an interpolation method described in detail in [30], and which we will also employ in the present work for four sets of parametrizations that will be detailed below in Table 1. This version of the nlNJL approach is denoted in the following as model B.

In spite of good results obtained for hybrid stars using the LOCV method for the hyperonic phase and model A of the nlNJL approach for the description of color superconducting quark matter, we note that the absence of a confining mechanism leads to rather low densities for the onset of the hadron-to-quark matter transition. In this situation it appears that the asymptotic EoS, i.e., hypernuclear matter in the low-density regime and quark matter in the high-density regime, cannot simply be trusted in the intermediate range of densities where a quark-hadron PT is expected. For this situation, it has been suggested to use an interpolation method [55, 56] between hadronic and quark matter models.

Table 1. Four different parameter sets which have been used for the interpolation of nlNJL model

Parameter	Set 1	Set 2	Set 3	Set 4
$\mu_<$, MeV	1090	1090	1090	1070
$\Gamma_<$, MeV	155	163	150	170
$\mu_\ll$, MeV	1500	1500	1500	1600
$\Gamma_\ll$, MeV	300	300	270	300
$\eta_<$	0.05	0.05	0.07	0.07
$\eta_>$	0.09	0.12	0.12	0.16
B, MeV/fm^3	30	30	20	25

In the present work, however, we will use model A with a Maxwell construction where it is applicable and not make use of the interpolation between quark and hadronic asymptotic EoS as described in [55]. Instead, we employ the interpolation technique of Ref. [57] which has also been used in [30] and is denoted here as model B. This method interpolates between different nlNJL parametrizations and thus corresponds to a density-dependent bag pressure as well as a density dependence of the repulsive vector meson coupling strength. For this model we investigated four sets of parametrizations for these density dependences and obtained for all of them an onset of deconfinement at densities above that for the onset of hyperons.

These different sets of parameters to interpolate the nlNJL EoS for numerical calculations of this work are given Table 1.

1.3. Phase Transition Construction. For constructing a first-order PT between hadronic phase and deconfined quark matter, we will apply here the Maxwell construction (MC) which assumes that both EoS should separately fulfill the charge-neutrality and β-equilibrium conditions with electrons and muons. Under such conditions the chemical potential of a particle species i can be written as

$$\mu_i = b_i \mu + q_i \mu_q, \tag{20}$$

where b_i is the baryon number of the species i, q_i denotes its charge in units of the electron charge, μ and μ_q are the baryonic and electric chemical potentials, respectively. The Gibbs conditions for phase equilibrium require that the temperatures, chemical potentials and pressures of the two phases should coincide at the phase transition:

$$\mu_H = \mu_Q = \mu_c, \tag{21}$$

$$T_H = T_Q = T_c, \tag{22}$$

$$P_H(\mu_B, \mu_e) = P_Q(\mu_B, \mu_e) = P_c. \tag{23}$$

In the above equations, the subscript c denotes the critical value of these thermodynamic variables for which chemical, thermal and mechanical phase equilibrium is established. In the present work, we construct the PT for the zero temperature case. Technically, one can plot the pressure as a function of chemical potential for two phases and merge them at the crossing point in which $P_{\mu_c} = P_c$. Physically, the phase with higher pressure (lower grand canonical potential) in a given chemical potential is considered out of PT region. We note that this setting of the problem inevitably evokes the so-called "reconfinement problem" [25,58]. In the present work, we will employ the "no reconfinement" paradigm which states that once the critical chemical potential for the deconfinement transition has been reached the "old" hadronic EoS will no longer be considered as a relevant alternative at still higher chemical potentials. Therefore, should a second crossing between hadronic and quark matter EoS occur in the pressure vs. chemical potential plane, it shall be ignored and thus a "reconfinement" will be excluded.

2. MASS–RADIUS RELATION FOR HYBRID STARS

A particularly interesting question in this context is the role which hyperons or deconfined quark matter can play in interpreting the observations of binary neutron star mergers. The observational constraints for maximum mass and radius of neutron star from the millisecond pulsar PSR J0740 + 6620 and the binary neutron star merger GW170817 should be fulfilled by the theoretical calculations. We have assumed the hybrid star is a hydrostatic equilibrated and spherically symmetric system. Thus, the mass–radius relation of the star can be determined by solving the well-known Tolman–Oppenheimer–Volkoff (TOV) equations [59, 60] for a given EoS,

$$
\frac{dP(r)}{dr} = -\frac{GM(r)\varepsilon(r)}{c^2 r^2} \times
$$
$$
\times \left(1 + \frac{P(r)}{\varepsilon(r)}\right) \left(1 + \frac{4\pi r^3 P(r)}{M(r)c^2}\right) \left(1 - \frac{2GM(r)}{rc^2}\right)^{-1}, \quad (24)
$$

$$
\frac{dM(r)}{dr} = \frac{4\pi\varepsilon(r)r^2}{c^2}. \quad (25)
$$

In these equations $P(r)$ and $\varepsilon(r)$ denote the pressure and the energy density profiles for the matter distribution in the CS interior, $M(r)$ is the cumulative mass enclosed in a spherical volume at the distance r from the center, and G is the gravitational constant. The gravitational mass $M = M(r = R)$ of the star is the mass enclosed within the radius of the star. By considering that the boundary condition $P(r = R) = 0$ defines the radius R for a chosen central energy density $\varepsilon_c = \varepsilon(r = 0)$, we have the necessary boundary and initial conditions to solve the TOV equations for a relativistic star with mass M and radius R, respectively. By increasing ε (or equivalently P) up to the maximum mass, the mass–radius relation can be obtained. For the EoS of the inner and outer crust of the neutron star, we use the results of Negele and Vautherin [61] and Harrison and Wheeler [62], respectively.

3. RESULTS

Figures 2 and 3 show the EoS for pressure as a function of chemical potential and energy density, respectively, for the Maxwell construction of the deconfinement phase transition. As can be seen in Fig. 3, the jump in energy density increases by decreasing the vector meson coupling parameter. However it is a big jump, but the crossing point occurs in low chemical potential which is before the onset of hyperons for $\eta \leqslant 0.14$.
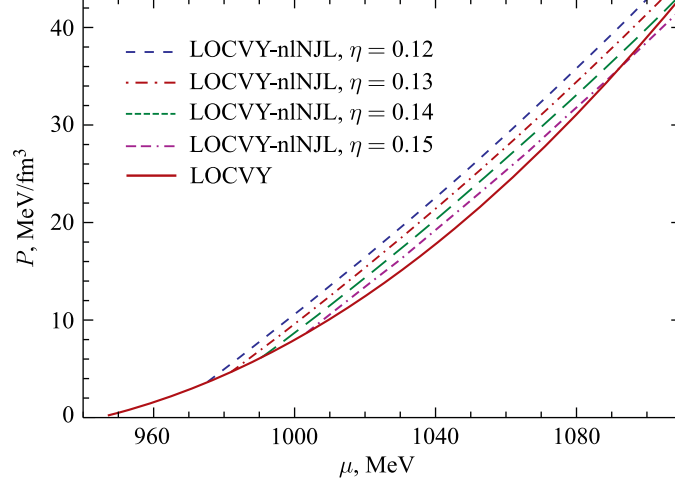
Fig. 2. Pressure as a function of chemical potential for the Maxwell construction of the deconfinement PT using the LOCV method with hyperons (LOCVY) for the hadronic phase and the color superconducting nlNJL model for quark matter
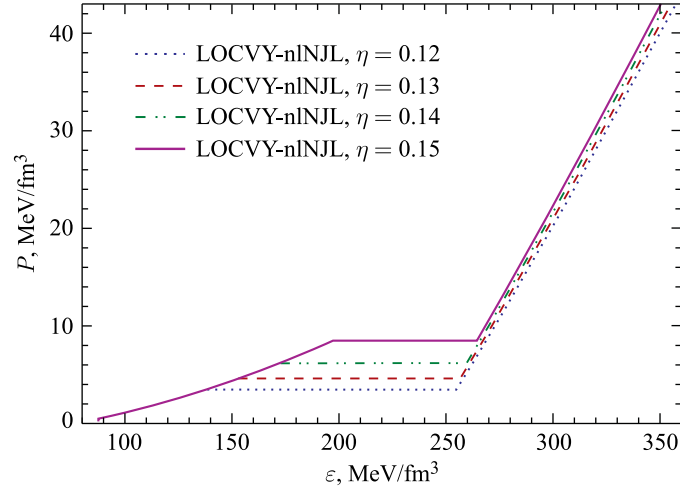
Fig. 3. Pressure as a function of energy density for the Maxwell construction of the deconfinement PT using the LOCV method with hyperons (LOCVY) for the hadronic phase and the color superconducting nlNJL model for quark matter

The gravitational mass of the hybrid star in the unit of solar mass has been plotted in Fig. 4 as a function of radius. As was mentioned before, we have considered the PT to quark matter as a solution for hyperon puzzle. As the figure

12
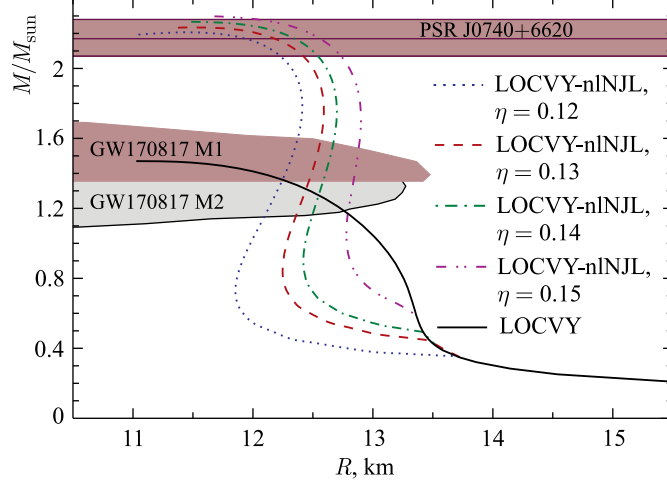
Fig. 4. Mass–radius relation of hybrid star for the Maxwell construction of the deconfinement PT using the LOCV method with hyperons (LOCVY) for the hadronic phase and the color superconducting nlNJL model for quark matter
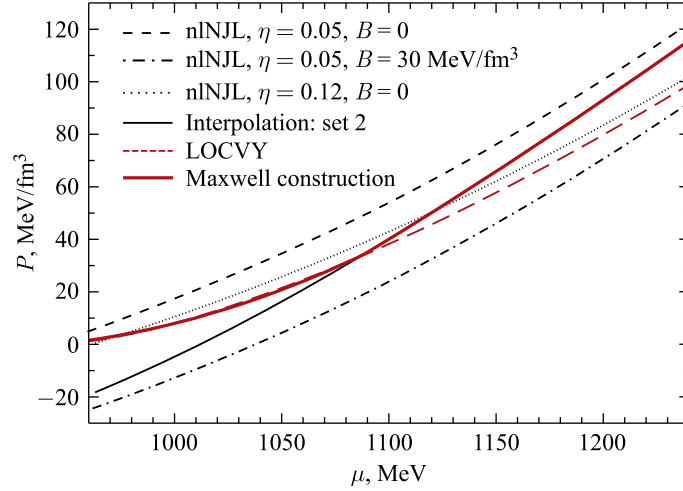
Fig. 5. Hybrid star EoS (black solid line) obtained by a Maxwell construction between the interpolated quark matter EoS for set 2 and the LOCVY EoS for hypernuclear matter in β-equilibrium with electrons, muons as well as Σ^- and Λ hyperons. The doubly interpolated quark matter EoS is based on three parametrizations of the nlNJL model: a soft (low η) one with confinement ($B \neq 0$) at low densities, a soft one without confinement ($B = 0$) at intermediate densities and a stiff one (high η) at high densities
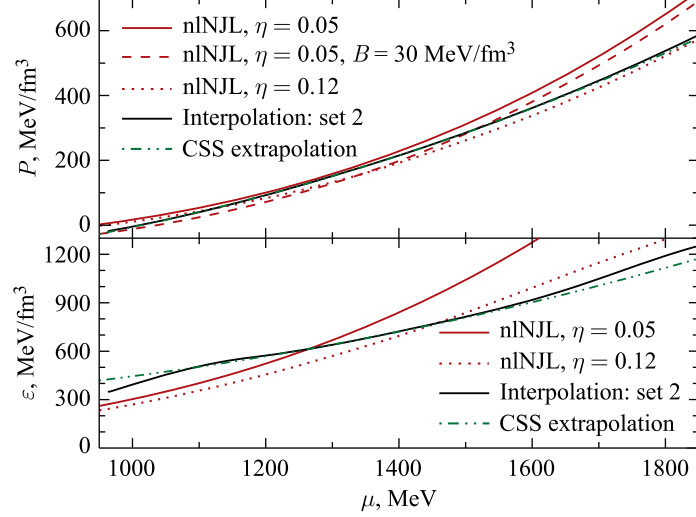
Fig. 6. Quark matter EoS in which we have used the interpolated EoS of set 2 at low and intermediate chemical potential, while for high chemical potential the CSS extrapolation method has been used. The parameters of the matching point are $\mu = 1539$ MeV and $\varepsilon = 851.4$ MeV/fm^3. The top panel shows the pressure as a function of the chemical potential in which there is a good agreement between interpolated EoS and extrapolated one. The lower plot shows the energy density as a function of chemical potential

shows, the PT which we have constructed not only increases the maximum mass for hybrid star, but also all of the EoS have fulfilled the observational constraint for the maximum mass of CS.

Figure 5 shows an example of the obtained EoS within this interpolation method for set 2 of the table. In this table the three initial nlNJL EoS for producing the interpolated EoS as well as LOCVY EoS and the PT EoS have been shown. The interpolated EoS can be considered as a generalized nonlocal chiral quark model EoS with the μ-dependent bag function $B(\mu)$ and vector coupling $\eta(\mu)$.

It is worth mentioning that for very high density, we have applied the constant speed of sound (CSS) extrapolation method to reach the maximum mass of hybrid stars. This technique can be considered as the lowest-order terms of a Taylor expansion of the quark matter EoS about the transition pressure [32]. An example of this extrapolation method for set 2 of the table is shown in Fig. 6. As can be seen in the figure, there is a good agreement between interpolated EoS and extrapolated one at high densities.

Figure 7 shows the squared speed of sound $c_s^2 = dP/d\varepsilon$ as a function of the energy density for all the sets in the table and that the CSS extrapolation

14
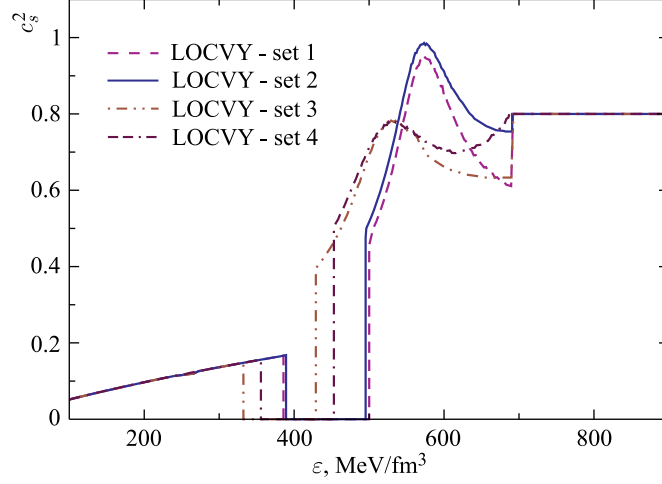
Fig. 7. The squared speed of sound c_s^2 in units of the squared speed of light as a function of the energy density for all the sets in the table. The region of high energy densities (> 700 MeV/fm^3) is described by a constant speed of sound model
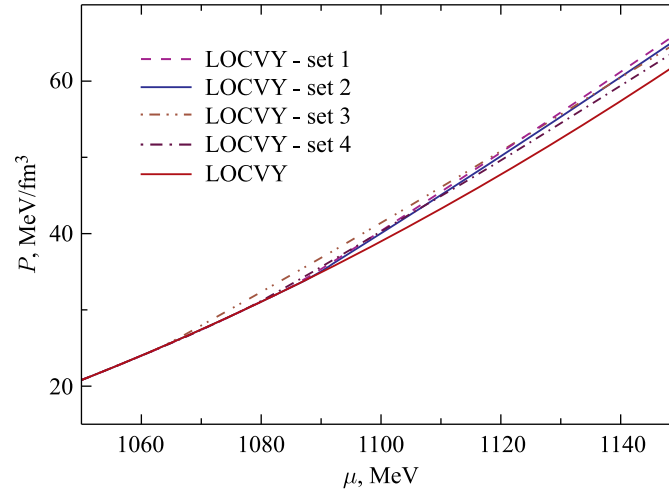
Fig. 8. Pressure as a function of chemical potential for the Maxwell construction of the deconfinement PT using the LOCV method for hypernuclear matter (LOCVY) and four sets of parametrization of model B for quark matter. The EoS of pure hypernuclear matter is shown as well

method has been used for them in high chemical potential to reach the maximum mass of hybrid star. The figure shows the regions of the first-order PT where c_s^2 in unit of the speed of light squared is equal to zero and fulfills the condition

15
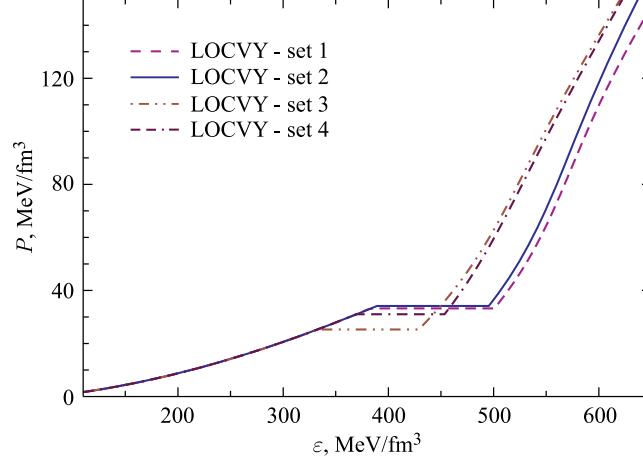
Fig. 9. Pressure as a function of energy density for the Maxwell construction of the deconfinement PT using the LOCV method for hypernuclear matter (LOCVY) and four sets of parametrization of model B for quark matter
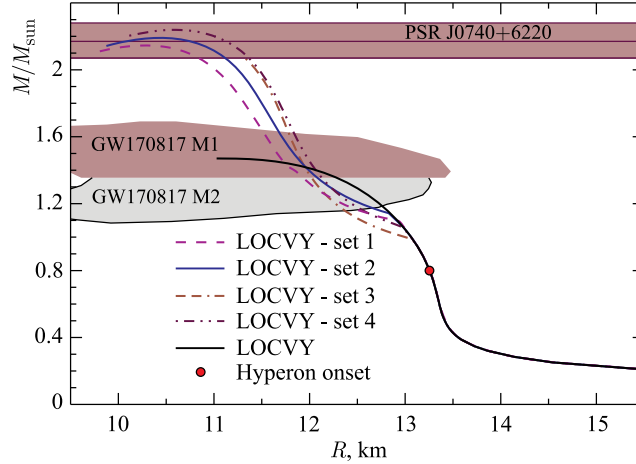
Fig. 10. Mass–radius relation of hybrid star for the Maxwell construction of the deconfinement PT using the LOCV method for hypernuclear matter (LOCVY) and four sets of parametrization of model B for quark matter. The hyperon onset (filled circle) occurs at a star mass of $0.8M_\odot$, before the quark deconfinement, so that above that mass there are hybrid stars with three phases of core matter: nuclear, hypernuclear and quark matter, see Fig. 11

of causality $c_s^2 < 1$ at all energy densities. One should note that the quark matter speed of sound is held constant after matching point. Figures 8 and 9 show the pressure as a function of chemical potential and energy density,
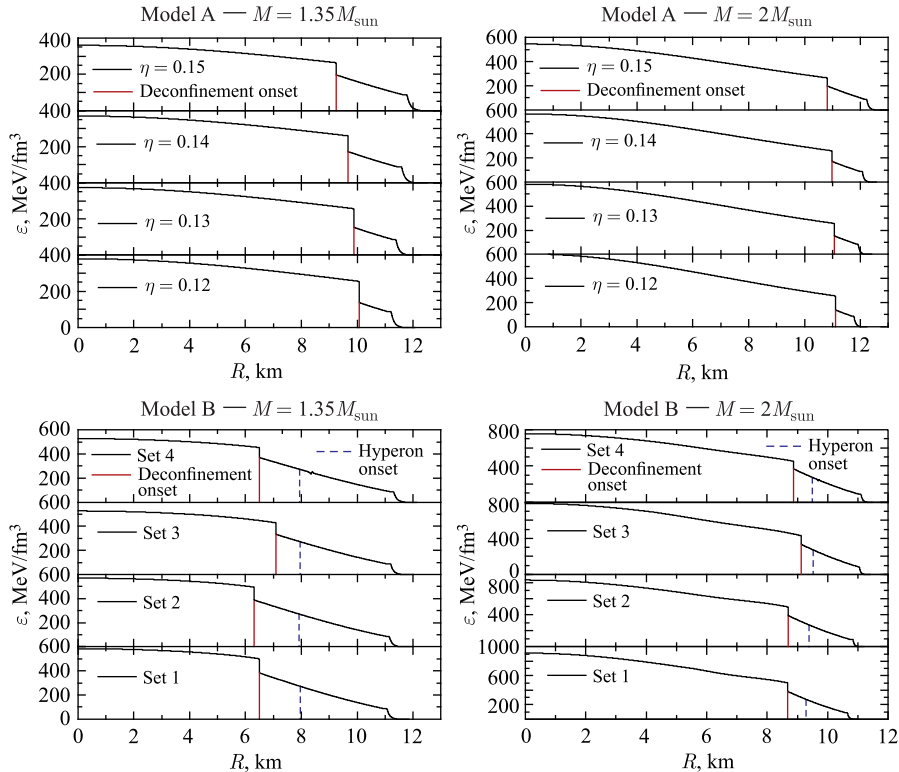
Fig. 11. Profiles of energy densities for model A (upper panels) with four cases of vector coupling strength $\eta = 0.12, 0.13, 0.14, 0.15$ and the four sets of parametrization of model B (lower panels) for the case of a typical binary radio pulsar mass of $1.35 M_\odot$ (left panels) and for the case of a high-mass pulsar with $2.0 M_\odot$ (right panels). While for all parametrizations of model A the deconfinement transition occurs directly from the nuclear matter outer core to the extended quark matter core, in model B there is a shell of hypernuclear matter in-between the inner core of superconducting quark matter and the outer core of nuclear matter

respectively, for the Maxwell construction of the deconfinement PT in which the LOCVY EoS for hypernuclear matter as well as the four sets of interpolated (with extrapolation at high chemical potential) EoS for quark matter have been used. The gravitational mass of the hybrid star in the unit of solar mass has been plotted in Fig. 10 as a function of radius. As shown in Figs. 8–10, by using the interpolation method of model B, we obtain a strong PT for which the onset of deconfinement takes place at a sufficiently large chemical potential so that there is an intermediate hypernuclear phase between the nuclear and the deconfined quark matter phases.
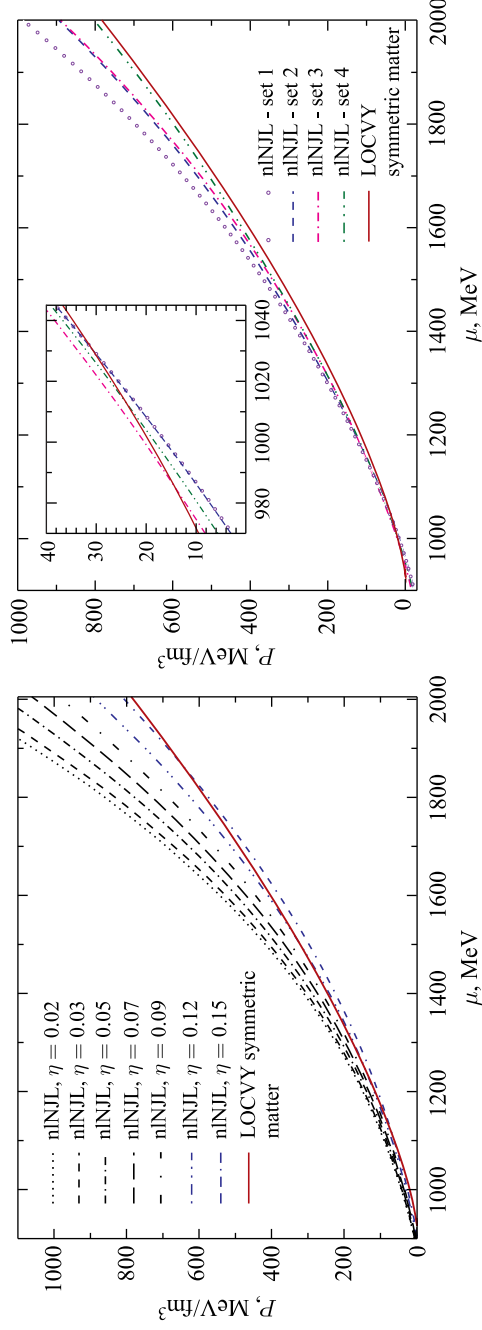
Fig. 12. Pressure versus baryochemical potential in the isospin-symmetric case for the LOCVY model of hypernuclear matter and for the nlNJL approach to quark matter. Left panel: model A with vector coupling strengths $\eta = 0.02, 0.03, 0.05, 0.07, 0.09, 0.12, 0.15$; right panel: model B for sets 1, 2, 3 and 4. For model A there is obviously a problem at low chemical potential, where due to the lack of confinement in this model the quark pressure is above the hadronic one. For the cases with $\eta > 0.12$ (which produce reasonable hybrid star EoS) there are also reasonable phase transitions when one ignores the region below $\mu \sim 1400$ MeV. For $\eta = 0.12$ the critical density for the onset of deconfinement is $n_c = 0.79$ fm^{-3} and for $\eta = 0.15$ it is $n_c = 0.98$ fm^{-3}. For model B under isospin-symmetric conditions all the considered parametrizations of sets 1–4 predict a deconfinement phase transition between $2.2n_0$ and $2.7n_0$. For a detailed discussion, see text

18

Furthermore, the obtained maximum masses obey the modern compact star constraints. It should be mentioned that in this case, the hypernuclear EoS is not soft enough at low densities so as to produce a sufficiently big jump in energy density to have the third family of CSs.

In Fig. 11 we show the profiles of energy densities for model A (upper panels) with four cases of vector coupling strength $\eta = 0.12, 0.13, 0.14, 0.15$ and the four sets of parametrization of model B (lower panels). In the left panels the case of a typical binary radio pulsar mass of $1.35 M_\odot$ is shown (which is relevant for scenarios explaining the binary merger GW170817), and in the right panels the case of a high-mass pulsar with $2.0 M_\odot$ is considered. While for all parametrizations of model A the deconfinement transition occurs directly from the nuclear matter outer core to the extended quark matter core, in model B there is a shell of hypernuclear matter in-between the inner core of superconducting quark matter and the outer core of nuclear matter.

Finally, in Fig. 12 we discuss the case of isospin-symmetric matter that is relevant for applications to relativistic heavy-ion collisions. We see that for model A (left panel) the cases with sufficiently repulsive vector meson mean field ($\eta > 0.12$) do predict a deconfinement transition at high densities beyond $0.79 \, \text{fm}^{-3}$. The transitions from quark to hadronic phase at lower densities are unphysical and shall be ignored. Their appearance may be attributed to the absence of a confining mechanism for quarks in model A. Less repulsive vector mean fields ($\eta \leqslant 0.09$) do not predict a deconfinement transition for the same reason. For model B (shown in the right panel of Fig. 12) all the considered parametrizations (sets 1–4) predict a deconfinement phase transition under isospin-symmetric conditions with onset densities between $2.2 n_0$ and $2.7 n_0$. Under compact star conditions these parametrizations of model B predict onset masses for quark deconfinement between $0.99 M_\odot$ and $1.14 M_\odot$ while fulfilling the maximum mass constraint and thus solving the hyperon puzzle. As a characterizing feature of this hybrid EoS model, there is an intermediate hypernuclear phase for all stars in the range of observed compact star masses.

CONCLUSIONS

We have reconsidered the problem that the appearance of hyperons softens the nuclear EoS such that under compact star conditions the constraint on the lower limit for the maximum mass at $2 M_\odot$ cannot be fulfilled (hyperon puzzle). To this end, we have applied a two-phase approach to hybrid compact star matter where the hadronic phase is described within the LOCV method including hyperons and the quark matter phase is modelled by a color superconducting nonlocal Nambu–Jona-Lasinio model with constant (model A) and with density-dependent (model B) coefficients. The phase transition has been obtained by a Maxwell construction. Our study confirms that also with the present set of modern equa-

tions of state the quark deconfinement presents a viable solution of the hyperon puzzle. A new finding of the present work is that model B allows for an intermediate hypernuclear matter phase in the hybrid star, between the nuclear and color superconducting quark matter phases, while in model A such a phase cannot be realized because the phase transition onset is at low densities, before the hyperon threshold density is passed.

We have discussed the possible application of the present hybrid EoS for estimating the onset density of the deconfinement phase transition in symmetric matter as it will be probed in future heavy-ion collision experiments at FAIR, NICA and corresponding energy scan programs at the CERN and RHIC facilities. We found that for model A the cases with a sufficiently strong repulsive vector mean field ($\eta > 0.12$) which produce reasonable hybrid star EoS have also a phase transition under isospin-symmetric conditions. For $\eta = 0.12$ the critical density is $n_c = 0.79$ fm^{-3} and for $\eta = 0.15$ it is $n_c = 0.98$ fm^{-3}. For the less repulsive vector mean fields ($\eta \leqslant 0.11$) there is no deconfinement transition in symmetric matter! This may be attributed to the absence of a confining mechanism for quarks in model A. For model B a density-dependent bag pressure serves as a confining mechanism at low densities. This model predicts a deconfinement phase transition under isospin-symmetric conditions for all the considered parametrizations (sets 1–4) at densities between $2.2n_0$ and $2.7n_0$. For these same parameter sets the hybrid star EoS predicts an onset of quark deconfinement for compact stars in the mass range from $0.99M_\odot$ to $1.14M_\odot$ while fulfilling the maximum mass constraint and thus solving the hyperon puzzle. It is remarkable that in this model all compact stars in the observed range of masses (i.e., from about $1.2M_\odot$ to $2.2M_\odot$) may have a shell of hypernuclear matter between the inner core of color superconducting quark matter and the outer core of nonstrange nuclear matter. Therefore, the scenarios of binary compact star mergers should consider the case of coalescing hybrid stars and investigate the role of hypernuclear and quark matter phases in this context.

The application of the quark-hadron hybrid EoS to binary merger simulations, however, requires the inclusion of finite temperatures which is planned for the future extension of the presented approach. On such a basis the recently suggested gravitational wave signal for a deconfinement transition [63] could then be discussed and the supernova explodability of blue supergiant stars [64] when described with the finite-temperature extension of the here introduced class of hybrid EoS could be investigated. To such a further development of the EoS would correspond a structure of the QCD phase diagram in the full space of variables, i.e., temperature, baryon density, and isospin asymmetry which besides astrophysical applications is of relevance for simulations of heavy-ion collision experiments.

REFERENCES

1. A. W. Steiner, J. M. Lattimer and E. F. Brown, Astrophys. J. **722** (2010) 33.
2. H. T. Cromartie *et al.*, Nat. Astron. **3** (2019) 439, arXiv: 1904.06759.
3. B. P. Abbott *et al.* [LIGO Scientific and Virgo Collaborations], Phys. Rev. Lett. **119** (2017) no.16, 161101.
4. A. Bauswein, O. Just, H. T. Janka and N. Stergioulas, Astrophys. J. **850** (2017) no.2, L34.
5. E. Annala, T. Gorda, A. Kurkela and A. Vuorinen, Phys. Rev. Lett. **120** (2018) no.17, 172703.
6. V. A. Ambartsumyan and G. S. Saakyan, Soviet Astronomy **4** (1960) no.2, 187.
7. M. Baldo, G. F. Burgio and H. J. Schulze, Phys. Rev. C **58** (1998) 3688.
8. M. Baldo, G. F. Burgio and H. J. Schulze, Phys. Rev. C **61** (2000) 055801.
9. M. Shahrbaf and H. R. Moshfegh, Annals Phys. **402** (2019) 66.
10. Y. Yamamoto, T. Furumoto, N. Yasutake and T. A. Rijken, Eur. Phys. J. A **52** (2016) no.2, 19
11. K. A. Maslov, E. E. Kolomeitsev and D. N. Voskresensky, Phys. Lett. B **748** (2015) 369.
12. K. A. Maslov, E. E. Kolomeitsev and D. N. Voskresensky, Nucl. Phys. A **950** (2016) 64.
13. C. Providéncia, M. Fortin, H. Pais and A. Rabhi, Front. Astron. Space Sci. **6** (2019) 13.
14. A. Drago, A. Lavagno, G. Pagliara and D. Pigato, Phys. Rev. C **90** (2014) no.6, 065809.
15. I. Vidaña, M. Bashkanov, D. P. Watts and A. Pastore, Phys. Lett. B **781** (2018) 112.
16. A. Mukherjee, S. Schramm, J. Steinheimer and V. Dexheimer, Astron. Astrophys. **608** (2017) A110.
17. M. Marczenko, D. Blaschke, K. Redlich and C. Sasaki, Phys. Rev. D **98** (2018) no.10, 103021.
18. M. Marczenko, D. Blaschke, K. Redlich and C. Sasaki, Universe **5** (2019) 180.
19. F. Weber, Prog. Part. Nucl. Phys. **54** (2005) 193.

20. G. F. Burgio, M. Baldo, P. K. Sahu and H. J. Schulze, Phys. Rev. C **66** (2002) 025802.

21. M. Baldo, G. F. Burgio and H.-J. Schulze, astro-ph/0312446.

22. T. Klähn, D. Blaschke, F. Sandin, C. Fuchs, A. Faessler, H. Grigorian, G. Röpke and J. Trümper, Phys. Lett. B **654** (2007) 170.

23. D. Blaschke, S. Fredriksson, H. Grigorian, A. M. Oztas and F. Sandin, Phys. Rev. D **72** (2005) 065020.

24. S. Typel, G. Röpke, T. Klähn, D. Blaschke and H. H. Wolter, Phys. Rev. C **81** (2010) 015803.

25. R. Lastowiecki, D. Blaschke, H. Grigorian and S. Typel, Acta Phys. Polon. Supp. **5** (2012) 535.

26. L. Bonanno and A. Sedrakian, Astron. Astrophys. **539** (2012) A16.

27. G. A. Lalazissis, J. König and P. Ring, Phys. Rev. C **55** (1997) 540.

28. G. A. Lalazissis, T. Niksic, D. Vretenar and P. Ring, Phys. Rev. C **71** (2005) 024312.

29. A. Ayriyan, D. Alvarez-Castillo, D. Blaschke and H. Grigorian, Universe **5** (2019) no.2, 61.

30. D. E. Alvarez-Castillo, D. B. Blaschke, A. G. Grunfeld and V. P. Pagura, Phys. Rev. D **99** (2019) no.6, 063010.

31. U. H. Gerlach, Phys. Rev. **172** (1968) 1325.

32. M. G. Alford, S. Han and M. Prakash, Phys. Rev. D **88** (2013) no.8, 083013.

33. N. K. Glendenning and C. Kettner, Astron. Astrophys. **353** (2000) L9.

34. D. Blaschke, D. E. Alvarez-Castillo and S. Benic, PoS **CPOD 2013** (2013) 063.

35. S. Benic, D. Blaschke, D. E. Alvarez-Castillo, T. Fischer and S. Typel, Astron. Astrophys. **577** (2015) A40.

36. D. E. Alvarez-Castillo and D. B. Blaschke, Phys. Rev. C **96** (2017) no.4, 045809.

37. J. C. Owen, R. F. Bishop and J. M. Irvine, Nucl. Phys. A **277** (1977) 45.

38. M. Modarres and J. M. Irvine, J. Phys. G **5** (1979) 511.

39. G. H. Bordbar and M. Modarres, Phys. Rev. C **57** (1998) 714.

40. M. Modarres and G. H. Bordbar, Phys. Rev. C **58** (1998) 2781.

41. M. Modarres and H. R. Moshfegh, Phys. Rev. C **62** (2000) 044308.

42. H. R. Moshfegh and M. Modarres, Nucl. Phys. A **759** (2005) 79.

43. H. R. Moshfegh and M. Modarres, Nucl. Phys. A **792** (2007) 201.

44. E. Hiyama, Y. Yamamoto, T. A. Rijken and T. Motoba, Phys. Rev. C **74** (2006) 054312.

45. E. Hiyama, M. Kamimura, T. Motoba, T. Yamada and Y. Yamamoto, Phys. Rev. C **66** (2002) 024007.

46. S. Goudarzi and H. R. Moshfegh, Phys. Rev. C **91** (2015) no.5, 054320, Erratum: [Phys. Rev. C **96** (2017) no.4, 049902].

47. S. Goudarzi and H. R. Moshfegh, Nucl. Phys. A **985** (2019) 1.

48. M. Modarres and H. R. Moshfegh, Physica A **388** (2009) 3297.

49. M. Modarres, H. R. Moshfegh, and A. Sepahvand, Eur. Phys. J. B **31** (2003) 159.

50. A. Akmal, V. R. Pandharipande and D. G. Ravenhall, Phys. Rev. C **58** (1998) 1804.

51. H. R. Moshfegh and S. Zaryouni, Eur. Phys. J. A **43** (2010) 283; **45** (2010) 69.

52. R. B. Wiringa, V. G. J. Stoks and R. Schiavilla, Phys. Rev. C **51** (1995) 38.

53. D. Gomez Dumm, D. B. Blaschke, A. G. Grunfeld and N. N. Scoccola, Phys. Rev. D **73** (2006) 114019.

54. D. B. Blaschke, D. Gomez Dumm, A. G. Grunfeld, T. Klähn and N. N. Scoccola, Phys. Rev. C **75** (2007) 065804.

55. K. Masuda, T. Hatsuda and T. Takatsuka, PTEP **2013** (2013) no.7, 073D01.

56. M. Asakawa and T. Hatsuda, Phys. Rev. D **55** (1997) 4488.

57. D. Blaschke, D. E. Alvarez Castillo, S. Benic, G. Contrera and R. Lastowiecki, PoS **ConfinementX** (2012) 249.

58. J. L. Zdunik and P. Haensel, Astron. Astrophys. **551** (2013) A61.

59. R. C. Tolman, Phys. Rev. **55** (1939) 364.

60. J. R. Oppenheimer and G. M. Volkoff, Phys. Rev. **55** (1939) 374.

61. J. W. Negele and D. Vautherin, Nucl. Phys. A **207** (1973) 298. doi:10.1016/0375-9474(73)90349-7.

62. B. K. Harrison, K. S. Thorne, M. Wakano, J. A. Wheeler, Gravitation Theory and Gravitational Collapse, University of Chicago Press, Chicago, 1965.

63. A. Bauswein, N. U. F. Bastian, D. B. Blaschke, K. Chatziioannou, J. A. Clark, T. Fischer and M. Oertel, Phys. Rev. Lett. **122** (2019) no.6, 061102.

64. T. Fischer *et al.*, Nat. Astron. **2** (2018) no.12, 980.

Редактор *Е. И. Кравченко*